

# Dalton Transactions

An international journal of inorganic chemistry

Accepted Manuscript

This article can be cited before page numbers have been issued, to do this please use: L. Verger, S. Chenu, J. Trébosc, S. Sundaramoorthy, A. Choudhury, O. Hernandez, E. Furet, D. Le Coq, L. Calvez and O. Lafon, *Dalton Trans.*, 2026, DOI: 10.1039/D6DT00232C.



This is an Accepted Manuscript, which has been through the Royal Society of Chemistry peer review process and has been accepted for publication.

Accepted Manuscripts are published online shortly after acceptance, before technical editing, formatting and proof reading. Using this free service, authors can make their results available to the community, in citable form, before we publish the edited article. We will replace this Accepted Manuscript with the edited and formatted Advance Article as soon as it is available.

You can find more information about Accepted Manuscripts in the [Information for Authors](#).

Please note that technical editing may introduce minor changes to the text and/or graphics, which may alter content. The journal's standard [Terms & Conditions](#) and the [Ethical guidelines](#) still apply. In no event shall the Royal Society of Chemistry be held responsible for any errors or omissions in this Accepted Manuscript or any consequences arising from the use of any information it contains.

# Synthesis of the $\text{NaGa}(\text{S}_{1-x}\text{Se}_x)_2$ solid solution from mechanically activated precursors

Louisiane Verger\*<sup>1</sup>, Julien Trébosc<sup>2</sup>, Santhoshkumar Sundaramoorthy<sup>3</sup>, Amitava Choudhury<sup>3</sup>,  
Olivier Hernandez<sup>4</sup>, Eric Furet<sup>1</sup>, Sébastien Chenu<sup>1</sup>, David Le Coq<sup>1</sup>, Laurent Calvez<sup>1</sup>, Olivier  
Lafon<sup>5</sup>

<sup>1</sup> Univ Rennes, CNRS, ISCR (Institut des Sciences Chimiques de Rennes) – UMR 6226, F-35000 Rennes, France

<sup>2</sup> Univ. Lille, CNRS, INRAE, Centrale Lille, Univ. Artois, FR 2638 – IMEC – Fédération Chevreul, 59000 Lille, France.

<sup>3</sup> Department of Chemistry, Missouri University of Science and Technology, Rolla, Missouri 65409, United States.

<sup>4</sup> Nantes Université, CNRS, Institut des Matériaux de Nantes Jean Rouxel, IMN, F-44000 Nantes, France.

<sup>5</sup> Univ. Lille, CNRS, Centrale Lille, Univ. Artois, UMR 8181 – UCCS – Unité de Catalyse et Chimie du Solide, 59000 Lille, France.

\**[louisiane.verger@univ-rennes.fr](mailto:louisiane.verger@univ-rennes.fr)*

## Abstract

$\text{NaGaS}_2$  and  $\text{NaGaSe}_2$  are two recently discovered compounds that crystallize in the same structure type. In this work,  $\text{NaGa}(\text{S}_{1-x}\text{Se}_x)_2$  ( $x = 0.5, 0.75$  and  $1$ ) are prepared by an alternative synthesis route, mechanochemistry followed by heat treatment.  $\text{Na}_2\text{S}$ ,  $\text{Na}_2\text{Se}$ ,  $\text{Ga}_2\text{S}_3$  and  $\text{Ga}_2\text{Se}_3$  are milled in stoichiometric proportions. Differential scanning calorimetry, X-ray diffraction and solid-state nuclear magnetic resonance ( $^{23}\text{Na}$  and  $^{71}\text{Ga}$ ) show that the compounds after milling are composed of crystalline  $\text{NaGa}(\text{S}_{1-x}\text{Se}_x)_2$  with an amorphous part. Annealing promotes the formation of crystalline  $\text{NaGa}(\text{S}_{1-x}\text{Se}_x)_2$ . A linear variation in the lattice parameters is observed, indicating that a solid solution is formed and that Se substitutes for S.



## 1. Introduction

View Article Online  
DOI: 10.1039/D6DT00232C

The need for safer rechargeable batteries with higher power densities is driving the search for all-solid-state battery (ASSB) designs using solid-state electrolytes (1). Furthermore, sodium-based inorganic ASSBs offer an alternative to lithium technologies for large-scale applications, thanks to their lower cost and the widespread availability of Na element. Solid-state electrolytes can be divided into four classes:  $\beta/\beta''$ - $\text{Al}_2\text{O}_3$ , NASICON, complex hydrides and halides and finally sulfides (2). The latter are widely studied due to their soft mechanical properties, which ensure good contact at electrolyte/electrode interfaces, low grain boundary resistance and higher ionic conductivity compared to their oxide counterparts.

Sulfide-based materials are generally synthesized in silica tubes sealed under vacuum, which poses two problems: the reactivity of sodium with silica and sulfur vapors. To overcome these problems, mechanochemistry is used, where precursors are milled at high energy, inducing a chemical reaction. Depending on the precursors and the milling conditions, the resulting material may be (i) amorphous, (ii) crystalline, or (iii) a composite with an amorphous part and a crystalline part. The synthesis route of amorphous sodium thiophosphates for solid-state electrolyte has been established through mechanochemistry by Noi *et al.* (3). Since then, many different  $\text{Na}^+$  conducting sulfur-based materials have been obtained by mechanochemistry, such as  $\text{Na}_3\text{BS}_3$  (4),  $\text{Na}_2\text{S-In}_2\text{S}_3$  (5),  $\text{Na}_5\text{AlS}_4\text{-Na}_4\text{SiS}_4$  (6),  $\text{Na}_6\text{MgS}_4$  (7) and  $\text{Na}_2\text{CaSnS}_4$  (8), in amorphous or crystalline forms. The amorphous domain of a given system can be extended by the use of mechanochemistry compared to melt-quenching (9), which could be due to higher quenching rate when impacting the beads with the powder (10). Heat treatments can be employed as a second step on the amorphous material to promote crystallization. In general, the crystalline phase is the one obtained by conventional high-temperature synthesis (11, 12). However, for some specific compositions, metastable phases can be obtained (13), such as  $\text{Li}_7\text{P}_3\text{S}_{11}$  or  $\text{Na}_3\text{PS}_4$  (14, 15).

Recently, we used mechanochemistry to extend the amorphous domain of the pseudo binary  $x[\text{Na}_2\text{S}] \cdot (100-x)[\text{Ga}_2\text{S}_3]$ , with  $\text{Na}_2\text{S}$  content ranging from  $x = 20$  to 80 (9). Crystalline  $\text{NaGaS}_2$  was obtained by heating amorphous  $\text{NaGaS}_2$  above its glass transition temperature (11). In parallel, crystalline  $\text{NaGaS}_2$  was synthesized for the first time by the flux method at 750 °C and 600 °C by Adhikary *et al.* and Klepov *et al.* (16, 17). The sodium selenogallate  $\text{NaGaSe}_2$  was later discovered, and is isostructural to its sulfide analogue  $\text{NaGaS}_2$  (18). They both crystallize in the  $C2/c$  space group according to a  $\text{TlGaSe}_2$  structure type. The structure is based on  $\text{Ga}_4\text{S}_{10}$  units connected by a bridging S atom, resulting in a layered structure. A representation of the



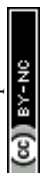
structure can be found in Supporting Information (SI), Figure S1. The  $\text{Ga}_4\text{S}_{10}$  units are composed of two pairs of  $\text{Ga}_2\text{S}_7$  connected through sharing corners.  $\text{Na}^+$  ions are located in the valley formed by the  $\text{Ga}_4\text{S}_{10}$  units, in prisms with triangular basis linked via their base to form chains. One prism on two is facing another prism of the upper plane, turned of  $90^\circ$ . There are two inequivalent sites for both Na and Ga elements.

In this work we use mechanochemistry followed by a thermal treatment to synthesis  $\text{NaGaSe}_2$ , and intermediate compositions along the solid solution  $\text{NaGa}(\text{S}_{1-x}\text{Se}_x)_2$ .

## 2. Experimental

$\text{NaGa}(\text{S}_{1-x}\text{Se}_x)_2$  ( $x = 0.5, 0.75$  and  $1$ ) were prepared by mechanochemical method using a planetary ball mill Pulverisette 7 (Fritsch).  $\text{Ga}_2\text{S}_3$  and  $\text{Ga}_2\text{Se}_3$  were firstly synthesized. 8 g of stoichiometric mixture of gallium (Neyco, 99.99 %) and sulfur (Strem Chemical Inc., 99.999 %) or selenium (Umicore, 5N), was ball milled during 4 hours at 400 rpm in a tungsten carbide (WC) vessel (internal volume of 45 mL) with 10 WC balls (diameter 10 mm) resulting in balls to powder mass ratio of 10:1 (19).  $\text{Na}_2\text{Se}$  was synthesized by taking stoichiometric amounts of Na and Se in liquid  $\text{NH}_3$  following Birch reduction techniques (20). The details of the synthesis can be found in the SI. Stoichiometric mixtures of  $\text{Ga}_2\text{S}_3$ ,  $\text{Ga}_2\text{Se}_3$ , and  $\text{Na}_2\text{S}$  (Alfa Aesar, 95% purity) were weighted for  $\text{NaGa}(\text{S}_{0.5}\text{Se}_{0.5})_2$ . Stoichiometric mixtures of  $\text{Ga}_2\text{Se}_3$ , and  $\text{Na}_2\text{S}$  (Alfa Aesar, 95% purity) were weighted for  $\text{NaGa}(\text{S}_{0.25}\text{Se}_{0.75})_2$ . And finally, stoichiometric mixtures of  $\text{Ga}_2\text{Se}_3$  and  $\text{Na}_2\text{Se}$  were weighted for  $\text{NaGaSe}_2$ . Each mixture was milled in zirconia pots (volume 45 mL), with zirconia balls (diameter 4 mm) and a 20:1 balls:powder mass ratio. The mass of the mixture was 5 g, and the rotational speed and milling duration were 600 rpm and 10 h, respectively. After 10 h of milling, the powders are yellow. The synthesis of the  $\text{NaGaSe}_2$  composition was performed twice to check the reproducibility of our method.

An annealing treatment was performed on powders obtained after mechanochemistry, pressed under 1.5 tons and under vacuum using a conventional uniaxial cold press to obtain a 1–1.5 mm thick pellet with a 10 mm diameter. The pellets were then heated in a silica tube sealed under vacuum, at their crystallization onset temperature  $T_x + 35^\circ\text{C}$  during 12 h. After annealing, the color of the powders becomes orange.



A DSC Q20 Thermal Analysis instrument was used to characterize the thermal properties of the synthesized materials. Measurements were performed from room temperature up to 500 °C with a heating rate of 10 °C/min on samples sealed under nitrogen in an aluminum crucible.

Conventional XRD measurements were performed on powders after different milling times to follow reaction processes on samples protected from air by a Kapton (polyimide) window. They were recorded in the 5–65° 2 $\theta$  range with a 0.0261° step size and a counting time of 400 s/step using a PANalytical X'Pert Pro diffractometer (Bragg–Brentano geometry, Cu-source, Ni-filter, K $\alpha$  radiation, 40 kV, 40 mA, PIXcel 1D detector).

XRD data on powders obtained after the annealing process were recorded with a counting time of 1200 s/step and on a wider range (5–130 ° 2 $\theta$ ) on powdered samples protected from air by a polycarbonate dome, which allows better airtightness. Le Bail profile refinements using the FullProf program were carried out (21).

Energy Dispersive Spectroscopy (EDS) analyses were collected on a JEOL JSM-IT 300 scanning electron microscope (SEM) using an acceleration voltage of 20 kV.

The Nuclear Magnetic Resonance (NMR) experiments were carried out in the NMR facility of the advanced characterization platform of the Chevreul institute. Quantitative one-dimensional (1D) <sup>23</sup>Na and <sup>71</sup>Ga NMR spectra were acquired at a static magnetic field  $B_0 = 28.2$  T using a Bruker BioSpin Avance NEO spectrometer and a narrow-bore hybrid NMR magnet built from both low-temperature and high-temperature superconductors equipped with 1.3 mm double-resonance (HX) magic-angle spinning (MAS) probe (22). Sodium-23 isotope is a spin-3/2 quadrupolar nucleus with a high natural abundance ( $NA$ ) of 100%, and moderate gyromagnetic ratio,  $\gamma(^{23}\text{Na}) \approx 0.265\gamma(^1\text{H})$ , and electric quadrupolar moment,  $eQ$ , with  $Q = 10.4$  fm<sup>2</sup>, whereas for <sup>71</sup>Ga isotope,  $NA = 39.89\%$ ,  $\gamma(^{71}\text{Ga}) \approx 0.306\gamma(^1\text{H})$  and  $Q = 10.4$  fm<sup>2</sup> (23). All samples were packed into zirconia rotor inside an argon-filled glovebox to prevent contact with moisture. The rotors were rotated at a MAS frequency of 50 kHz. The 1D <sup>23</sup>Na and <sup>71</sup>Ga NMR spectra were acquired using Bloch-decay experiment using a pulse length,  $\tau_p = 1$   $\mu$ s, a radiofrequency (rf) field strength,  $\nu_1 = 90$  kHz for <sup>23</sup>Na, and  $\tau_p = 0.475$   $\mu$ s and  $\nu_1 = 128$  kHz for <sup>71</sup>Ga. The 1D <sup>23</sup>Na and <sup>71</sup>Ga NMR spectra result from averaging 512 and 1024 transients with a recycling delay of 3 s and 0.5 s for <sup>23</sup>Na and <sup>71</sup>Ga, respectively. The <sup>1</sup>H isotropic chemical shifts were referenced to tetramethylsilane (TMS) diluted at 1% vol. in CDCl<sub>3</sub> using the unresolved signal of adamantane at 1.73 ppm as a secondary reference. <sup>23</sup>Na and <sup>71</sup>Ga chemical shifts were indirectly referenced using the previously published relative NMR frequencies (23).



### 3. Results and discussion

The reaction during the milling procedure is followed by XRD measurements acquired on the powder after every hour. As an example, **Fig. 1a** shows the copper-source XRD patterns of the composition  $\text{NaGa}(\text{S}_{0.25}\text{Se}_{0.75})_2$  after 1, 2, 4, 6 and 10 h of milling the  $\text{Na}_2\text{S}$  and  $\text{Ga}_2\text{Se}_3$  precursors. The diffraction halo between  $15$  and  $25^\circ 2\theta$  is due to the Kapton window used to protect the sample from air. After 1 h and 2 h of milling, the sharp peaks of  $\text{Na}_2\text{S}$  and the broad peaks of  $\text{Ga}_2\text{Se}_3$  are still detected, together with a new phase crystallizing indicated by grey dots. After only 4 h of milling, the precursors are no longer detected, and additional peaks of the new phase are detected. The XRD patterns did not evolve between 6 and 10 h, so the mechanical process was stopped after 10 h. A similar evolution is observed for sample  $\text{NaGa}(\text{S}_{0.5}\text{Se}_{0.5})_2$ , presented in SI Figure S3. For  $\text{NaGaSe}_2$ , also shown in Figure S3 of the SI, the only different is the formation of an intermediate crystalline phase at 1 h and 2 h of milling, which then reacts. This phase is not present in the precursors, and remains unidentified.

**Fig. 1b** shows the copper-source XRD patterns of the  $\text{NaGa}(\text{S}_{1-x}\text{Se}_x)_2$  ( $x = 0.5, 0.75$  and  $1$ ) samples after 10 h of milling. The samples are poorly crystallized, with peaks that can be attributed to a unique  $\text{NaGa}(\text{S}_{1-x}\text{Se}_x)_2$  crystalline phase. S can be substituted by Se in the  $\text{NaGaS}_2$  structure and a solid solution therefore exists in the system  $\text{NaGa}(\text{S}_{1-x}\text{Se}_x)_2$ . They are shifted towards lower angles as the Se content increases. Contrary to our previous work on  $\text{NaGaS}_2$  ( $x = 0$ ), amorphous powders were not obtained during the ball-milling process due to the crystallization of  $\text{NaGa}(\text{S}_{1-x}\text{Se}_x)_2$  that could not be further totally amorphized. The samples are then a composite of a crystalline phase, and an amorphous part.



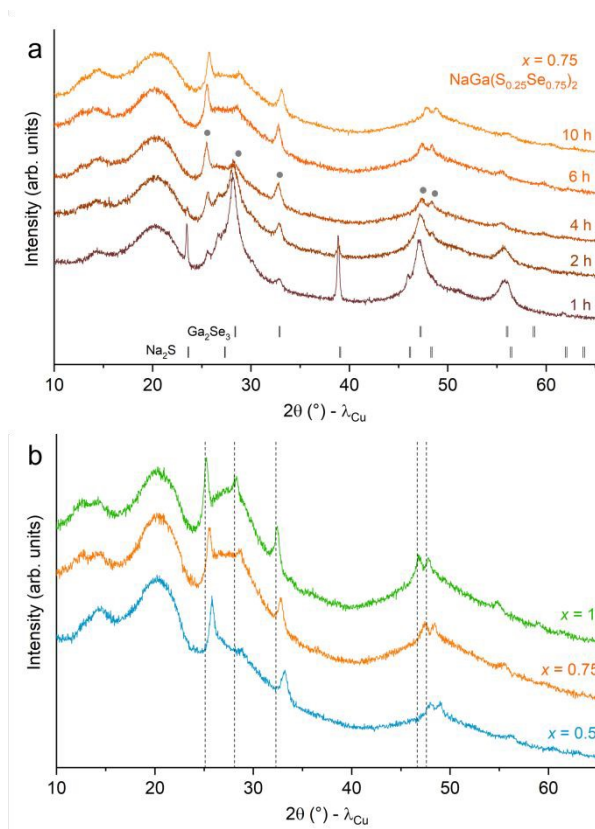


**Figure 1.** (a) Powder Cu-XRD patterns of the  $\text{NaGa}(\text{S}_{0.25}\text{Se}_{0.75})_2$  sample prepared by ball milling for different durations. The black vertical tick marks show Bragg positions of  $\text{Na}_2\text{S}$  and  $\text{Ga}_2\text{Se}_3$ . The grey dots correspond to crystalline  $\text{NaGa}(\text{S}_{0.25}\text{Se}_{0.75})_2$ . (b) Powder Cu-XRD patterns of the  $\text{NaGa}(\text{S}_{1-x}\text{Se}_x)_2$  samples with  $x = 0.5$  (blue),  $0.75$  (green) and  $1$  (black) obtained after 10 h of milling. The vertical lines are guides for the eye to see the shift of the peaks.

**Fig. 2** shows the DSC traces for the  $\text{NaGa}(\text{S}_{1-x}\text{Se}_x)_2$  samples with  $x = 0.5$  (blue),  $0.75$  (green) and  $1$  (black) obtained after 10 h of milling. There was no clear evidence of the presence of a glass transition temperature attesting the presence of a glass. However, a crystallization peak is detected, shifted towards lower temperature with increasing the Se content in the samples. In the literature, the substitution of S by Se also induces a decrease in crystallization temperature in the Ga–Ge–X and Ga–Sb–X systems, where  $X = \text{S}$  or  $\text{Se}$  (24–27). The crystallization onset temperature ( $T_x$ ) is at 353, 334 and 322 °C (+/- 2 °C) for  $x = 0.5$ ,  $0.75$  and  $1$ , respectively.



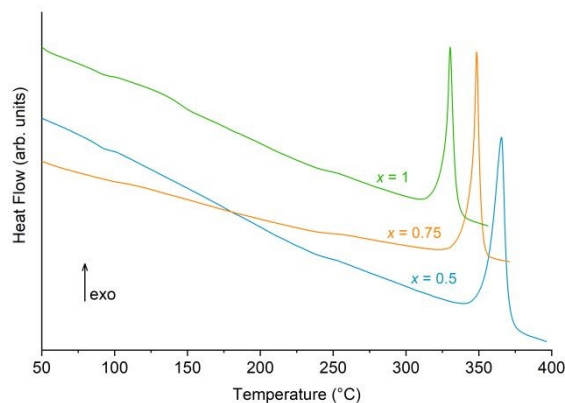


**Figure 2.** DSC curve of the  $\text{NaGa}(\text{S}_{1-x}\text{Se}_x)_2$  samples with  $x = 0.5$  (blue),  $0.75$  (green) and  $1$  (black) obtained after mechanical milling.

An annealing treatment was performed on the samples obtained after the mechanical milling at  $T_x + 35$  °C during 12 h. The crystallization of  $\text{NaGa}(\text{S}_{1-x}\text{Se}_x)_2$  is promoted by the thermal treatment, and  $\text{NaGa}(\text{S}_{1-x}\text{Se}_x)_2$  is the only crystalline phase detected with a higher crystallinity than before thermal treatment. For example, **Fig. 3** shows the XRD pattern of  $\text{NaGaSe}_2$  annealed during 12 h. The diffraction halo around  $18^\circ 2\theta$  is due to the polycarbonate dome used to protect the sample from air. The experimental patterns differ from the calculated one from the work of Adhikary *et al.* (16) and Balijapelly *et al.* (18) on  $\text{NaGaS}_2$  and  $\text{NaGaSe}_2$ , respectively. This is due to the presence of stacking faults in the structure which greatly affect the intensity and broadening of some reflections, leading to apparent observed extinctions. Possibilities to perform a Rietveld refinement are then extremely limited, but profile refinements using the Le Bail method without structural constraints were carried out.

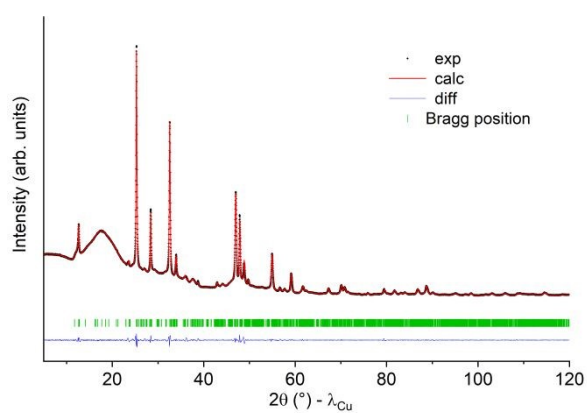


**Figure 3.** Powder Cu-XRD pattern of  $\text{NaGaSe}_2$  after annealing (black circles) and calculated profile using the Le Bail refinement method ( $\chi^2 = 5$ ,  $R_{wp} = 6.33\%$ ,  $R_p = 8.72\%$ ) (red line). The difference is



drawn in blue, green bars corresponds to the Bragg reflections for NaGaSe<sub>2</sub> from the structural model of Balijapelly *et al.* (18). View Article Online  
DOI: 10.1039/D6DT00232C

The refined lattice parameters of phases NaGa(S<sub>1-x</sub>Se<sub>x</sub>)<sub>2</sub> with  $x = 0.5, 0.75$  and  $1$  using the C2/c space group are gathered in **Fig. 4** and **Table 1**, together with data from the literature on NaGaS<sub>2</sub> and NaGaSe<sub>2</sub>. As expected, the lattice parameters increase with the substitution of S by Se.  $a$  and  $b$  from NaGaSe<sub>2</sub> obtained by mechanochemistry and thermal treatment are closed to the one obtained by Balijapelly *et al.* (18). The  $c$  parameter is 0.07 Å lower in our work, meaning that the distance between the layer is lower. A linear regression points out that the solid solution NaGa(S<sub>1-x</sub>Se<sub>x</sub>)<sub>2</sub> obeys Vegard's law.

**Table 1.** Lattice parameters of NaGa(S<sub>1-x</sub>Se<sub>x</sub>)<sub>2</sub> ( $x = 0, 0.5, 0.75$  and  $1$ ) from the literature and this work.

Composition	NaGaS <sub>2</sub>	NaGaS <sub>2</sub>	NaGa(S <sub>0.5</sub> Se <sub>0.5</sub> ) <sub>2</sub>	NaGa(S <sub>0.25</sub> Se <sub>0.75</sub> ) <sub>2</sub>	NaGaSe <sub>2</sub>	NaGaSe <sub>2</sub>
Reference	(16)	(11)	This work	This work	This work	(18)
$a$ (Å)	10.226(3)	10.214(3)	10.461(2)	10.554(9)	10.721(8)	10.738(3)
$b$ (Å)	10.227(3)	10.233(3)	10.494(1)	10.678(1)	10.769(9)	10.750(3)
$c$ (Å)	13.506(5)	13.537(3)	13.876(2)	14.035(2)	14.081(1)	14.152(4)
$\beta$ (°)	100.954(5)	101.054(2)	100.698(1)	100.669(6)	100.429(6)	100.954(5)

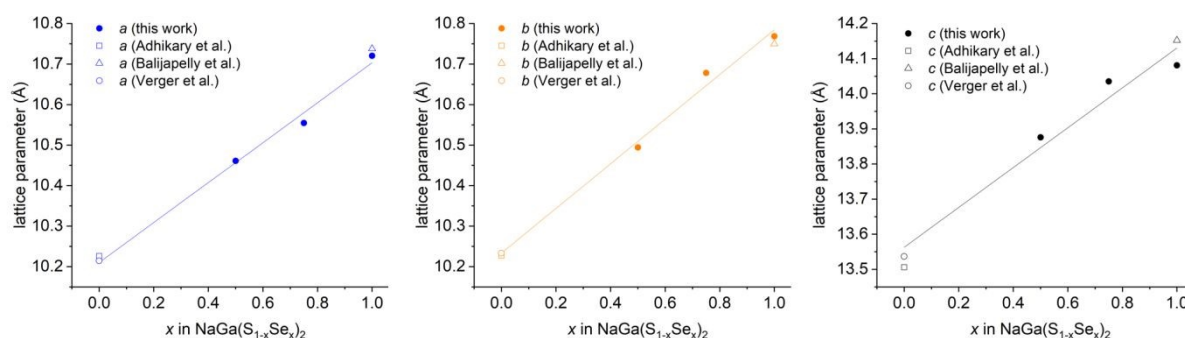


**Figure 4.** From left to right: evolution of  $a$ ,  $b$  and  $c$  lattice parameters as a function of  $x$  in NaGa(S<sub>1-x</sub>Se<sub>x</sub>)<sub>2</sub> (solid circles) synthesized in this work. The lines correspond to a linear fit using the data on compounds obtained by mechanochemistry from this work, and from our previously published work on NaGaS<sub>2</sub> (11) ( $R^2=0.99135, 0.99145, 0.96121$  for  $a, b$  and  $c$ , respectively).



The composition of the samples before and after thermal treatment is verified by EDS measurements and presented in **Table 2**. The  $K_{\alpha}$  radiation for Na (1.041 keV) and the  $L_{\alpha}$  radiation for Ga (1.098 keV) are close in energy and are therefore difficult to distinguish. This introduces an error: for all samples, the experimental quantitative analysis is systematically lower than the theoretical value for Na, and higher than the theoretical value for Ga. However, the measurements still show that the composition of the samples before and after annealing is similar and that the S/Se ratio is correct.

**Table 2:** Theoretical composition and composition evaluated by EDS ( $\pm 2$  at.%) of  $\text{NaGa}(\text{S}_{1-x}\text{Se}_x)_2$  sample after milling and after annealing.

		Na (at. %)	S (at. %)	Ga (at. %)	Se (at. %)
$x = 0.5$	After milling	18	19	37	26
	After annealing	19	20	35	26
	<i>Theoretical composition</i>	25	25	25	25
$x = 0.75$	After milling	18	9	35	37
	After annealing	19	10	33	38
	<i>Theoretical composition</i>	25	12.5	25	37.5
$x = 1$	After milling	17	0	35	48
	After annealing	17	0	33	49
	<i>Theoretical composition</i>	25	0	25	50

NMR spectroscopy was used to probe local environments of Na and Ga atoms. The quantitative 1D  $^{71}\text{Ga}$  spectra of the samples before and after the annealing treatment are shown in **Fig. 5**. Overall, the spectra of samples before the annealing treatment in dotted lines (just after the mechanochemical step) exhibit broader signals, betraying a distribution in local Ga environments typical of amorphous or poorly crystallized materials. The detected peaks become sharper after the annealing step, which leads to the crystallization of the materials and hence, reduces the disorder. The  $^{71}\text{Ga}$  NMR spectrum of  $\text{NaGa}(\text{S}_{0.5}\text{Se}_{0.5})_2$  exhibits five peaks, which can be attributed to Ga atoms covalently bonded to different numbers of S and Se atoms:  $\text{GaS}_4$ ,  $\text{GaSeS}_3$ ,  $\text{GaSe}_2\text{S}_2$ ,  $\text{GaSe}_3\text{S}$  and  $\text{GaSe}_4$ . In our previous work on  $\text{NaGaS}_2$ , we showed that the  $[\text{GaS}_4]$  sites resonated at an isotropic chemical shift of around 318 ppm and the two crystallographically inequivalent  $\text{GaS}_4$  sites are too similar to allow an unambiguous assignment (11). The peak with highest shift in the spectrum of  $\text{NaGa}(\text{S}_{0.5}\text{Se}_{0.5})_2$  can then be attributed to Ga surrounded by four S. As S is replaced by Se in  $[\text{GaX}_4]$  tetrahedron, the isotropic chemical shift of  $^{71}\text{Ga}$  nuclei is shifted towards lower values, down to about 170 ppm



for  $[\text{GaSe}_4]$ . Contrary to  $\text{NaGaS}_2$ , two distinct peaks are detected in  $\text{NaGaSe}_2$  after the thermal treatment, meaning that the two inequivalent sites for Ga can be distinguished.

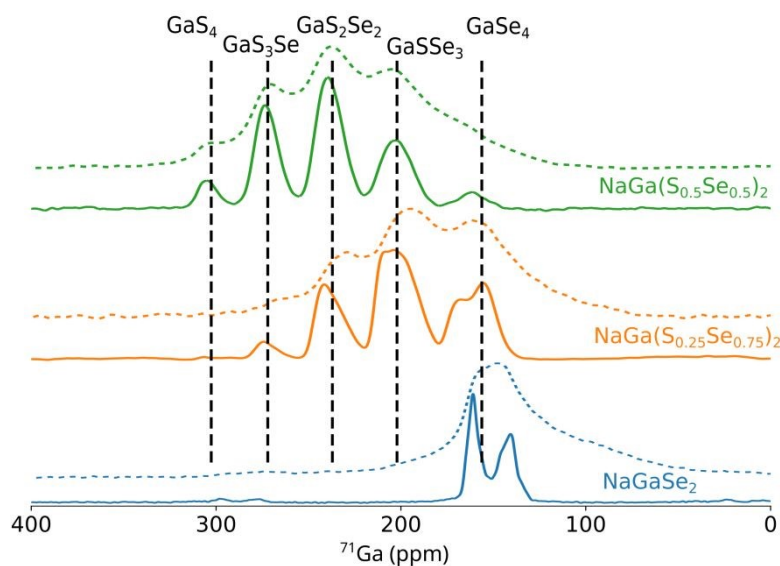


**Figure 5.** Quantitative 1D  $^{71}\text{Ga}$  MAS NMR spectra of  $\text{NaGa}(\text{S}_{1-x}\text{Se}_x)_2$  before (dashed line) and after the annealing treatment (solid line) acquired at 28.2 T.

The quantitative 1D  $^{23}\text{Na}$  MAS NMR spectra of the investigated samples are displayed on **Fig. 6**. The spectrum of  $\text{NaGa}(\text{S}_{0.5}\text{Se}_{0.5})_2$  before the thermal treatment (dotted green line in **Fig. 6**) are composed of two broad signals, one more intense at higher chemical shift (4.3 ppm) and a smaller contribution at lower chemical shift (-6.1 ppm). After annealing, the spectrum is composed only of the contribution at lower chemical shift, which becomes sharper. This change was also observed in our previous work on  $\text{NaGaS}_2$  (11). We can then conclude that the contribution at -6.1 ppm stems from crystalline  $\text{NaGa}(\text{S}_{0.5}\text{Se}_{0.5})_2$  phase, with the two inequivalent crystallographic Na sites overlapping, whereas the contribution at 4.3 ppm is produced by the amorphous phase. This assignment is in agreement with the XRD and DSC results, confirming that  $\text{NaGa}(\text{S}_{0.5}\text{Se}_{0.5})_2$  before the thermal treatment is a composite of a crystalline phase, and an amorphous part. Similar observations can be made on  $\text{NaGa}(\text{S}_{0.25}\text{Se}_{0.75})_2$  before the thermal treatment (dotted orange lines in **Fig. 6**), with one peak at 3.6 ppm attributed to amorphous phase, and one peak at -5.0 ppm assigned to crystalline  $\text{NaGa}(\text{S}_{0.25}\text{Se}_{0.75})_2$  phase. After the thermal treatment, one main signal centered at -7 ppm is detected, subsuming several contributions. The shoulder at -2.5 ppm probably corresponds to a residual amorphous phase. Finally, for the sample  $\text{NaGaSe}_2$  before thermal treatment, the spectrum is composed of one main contribution at 3.5 ppm, corresponding to amorphous



NaGaSe<sub>2</sub>, and two contributions at high chemical shift, -4.8 and -10 ppm. After crystallization, the spectrum is characterized by four peaks, while only two inequivalent sites for Na are reported in the structure. The synthesis was done a second time and the same spectrum was obtained. The attribution of the different features is still under investigation.

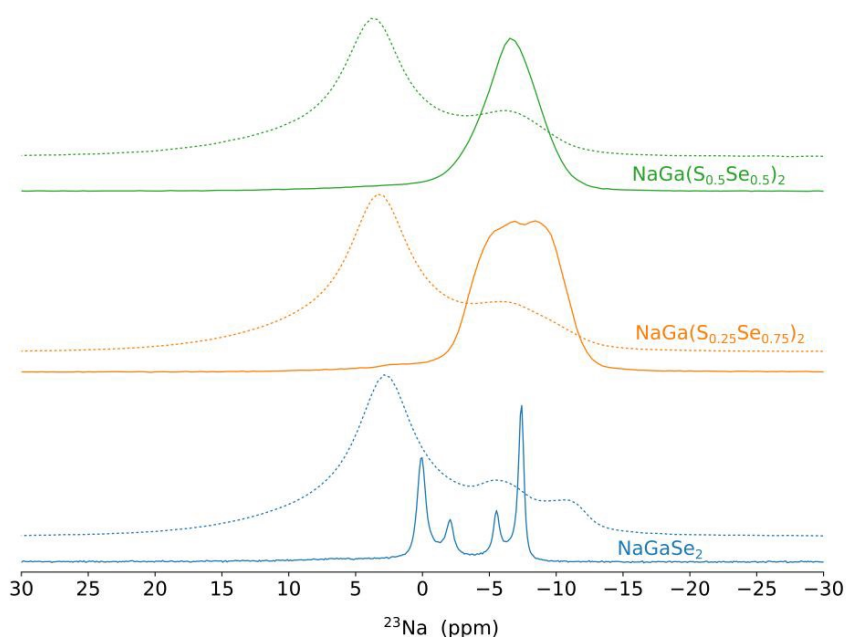
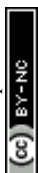


**Figure 6.** Quantitative 1D <sup>23</sup>Na MAS NMR spectra of NaGa(S<sub>1-x</sub>Se<sub>x</sub>)<sub>2</sub> before (dashed line) and after the annealing treatment (solid line).

## Conclusion

NaGa(S<sub>1-x</sub>Se<sub>x</sub>)<sub>2</sub> ( $x=0.5, 0.75$  and  $1$ ) was obtained by mechanochemistry. After 10 h of milling, the synthesized samples were characterized by XRD showing diffraction halos characteristic of amorphous materials, together with the presence of crystalline NaGa(S<sub>1-x</sub>Se<sub>x</sub>)<sub>2</sub>. The DSC traces show the presence of a crystallization peak, whose temperature decreases with increasing Se content. <sup>23</sup>Na NMR measurements confirmed the presence of crystalline and amorphous NaGa(S<sub>1-x</sub>Se<sub>x</sub>)<sub>2</sub> in the samples. An annealing treatment at  $T_x + 35$  °C was performed. This promotes the crystallization of NaGa(S<sub>1-x</sub>Se<sub>x</sub>)<sub>2</sub>. A linear variation of the lattice parameters is observed, which means that a solid solution is formed. Milling acts here at an activation step to promote the crystallization of NaGa(S<sub>1-x</sub>Se<sub>x</sub>)<sub>2</sub> at lower temperatures compared to classical synthesis in sealed silica tube.



## Conflicts of interest

There are no conflicts to declare.

## Data availability

The data supporting this article are available within the article, in the supplementary information (SI) and from the corresponding author upon request.

## Acknowledgments

This publication is (partially) supported by the European Union through the European Regional Development Fund (ERDF), the Ministry of Higher Education and Research, the French region of Brittany and Rennes Métropole. The Chevreul Institute is thanked for supporting CPER projects funded by the “Ministère de l’Enseignement Supérieur et de la Recherche”, the region “Hauts-DEER-France”, the ERDF program of the European Union and the “Métropole Européenne de Lille”. Financial support from the IR INFRANALYTICS FR2054 for conducting the research is gratefully acknowledged. We are grateful to Z. Barbotin for her help with the EDS measurements.

## References

1. M. Armand, J. M. Tarascon, Building better batteries. *Nature* **451**, 652-657 (2008).
2. Y. Yang *et al.*, Inorganic All-Solid-State Sodium Batteries: Electrolyte Designing and Interface Engineering. *Advanced Materials* **36**, 2308332 (2024).
3. K. Noi, A. Hayashi, M. Tatsumisago, Structure and properties of the Na<sub>2</sub>S–P<sub>2</sub>S<sub>5</sub> glasses and glass–ceramics prepared by mechanical milling. *Journal of Power Sources* **269**, 260-265 (2014).
4. F. Tsuji *et al.*, Preparation and characterization of sodium-ion conductive Na<sub>3</sub>BS<sub>3</sub> glass and glass–ceramic electrolytes. *Materials Advances* **2**, 1676-1682 (2021).
5. K. Motohashi *et al.*, Sodium-Ion Conducting Solid Electrolytes in the Na<sub>2</sub>S–In<sub>2</sub>S<sub>3</sub> System. *Electrochemistry* **90**, 067009-067009 (2022).
6. S. Harm *et al.*, Finding the Right Blend: Interplay Between Structure and Sodium Ion Conductivity in the System Na<sub>5</sub>AlS<sub>4</sub>–Na<sub>4</sub>SiS<sub>4</sub>. *Frontiers in Chemistry* **8**, (2020).
7. H. Ben Yahia, K. Motohashi, A. Sakuda, A. Hayashi, Mechanochemical Synthesis and Structure of the Alkali Metal Magnesium Chalcogenide Na<sub>6</sub>MgS<sub>4</sub>. *Inorganic Chemistry* **62**, 10440-10449 (2023).
8. H. Ben Yahia, A. Sakuda, A. Hayashi, Mechanochemical synthesis of rock salt-type Na<sub>2</sub>CaSnS<sub>4</sub> as a sodium-ion conductor. *RSC Mechanochemistry* **2**, 159-164 (2025).
9. K. Dénoue *et al.*, New synthesis route for glasses and glass-ceramics in the Ga<sub>2</sub>S<sub>3</sub>–Na<sub>2</sub>S binary system. *Materials Research Bulletin* **142**, 111423-111423 (2021).



10. B. Xue, L. Calvez, M. Allix, G. Delaizir, X. H. Zhang, Amorphization by Mechanical Milling for Making IR Transparent Glass-Ceramics. *Journal of the American Ceramic Society* **99**, 1573-1578 (2016). New Article Online  
DOI: 10.1039/D6DT00232C
11. L. Verger *et al.*, Mechanochemical synthesis and study of the local structure of NaGaS<sub>2</sub> glass and glass-ceramics. *Inorganic chemistry* **61**, 18476-18485 (2022).
12. C. Fritsch, A. L. Hansen, S. Indris, M. Knapp, H. Ehrenberg, Mechanochemical synthesis of amorphous and crystalline Na<sub>2</sub>P<sub>2</sub>S<sub>6</sub>-elucidation of local structural changes by X-ray total scattering and NMR. *Dalton Transactions* **49**, 1668-1673 (2020).
13. X. Zhi, A. R. West, Mechanochemical synthesis of Disordered Rock Salt Structures: Thermodynamic and Kinetic Considerations. *Chemistry of Materials* **12**, 25-25 (2023).
14. F. Mizuno, A. Hayashi, K. Tadanaga, M. Tatsumisago, New, Highly Ion-Conductive Crystals Precipitated from Li<sub>2</sub>S-P<sub>2</sub>S<sub>5</sub> Glasses. *Advanced Materials* **17**, 918-921 (2005).
15. A. Hayashi, K. Noi, A. Sakuda, M. Tatsumisago, Superionic glass-ceramic electrolytes for room-temperature rechargeable sodium batteries. *Nature Communications* **3**, 856-856 (2012).
16. A. Adhikary *et al.*, Unusual Atmospheric Water Trapping and Water Induced Reversible Restacking of 2D Gallium Sulfide Layers in NaGaS<sub>2</sub> Formed by Supertetrahedral Building Unit. *Chemistry of Materials* **32**, 5589-5603 (2020).
17. V. V. Klepov *et al.*, NaGaS<sub>2</sub>: An Elusive Layered Compound with Dynamic Water Absorption and Wide-Ranging Ion-Exchange Properties. *Angewandte Chemie International Edition* **59**, 10836-10841 (2020).
18. S. Balijapelly *et al.*, NaGaSe<sub>2</sub>: A Water-Loving Multifunctional Non-van der Waals Layered Selenogallate. *Inorganic Chemistry* **62**, 3886-3895 (2023).
19. K. Dénoue *et al.*, Mechanochemical synthesis and structural characterization of gallium sulfide Ga<sub>2</sub>S<sub>3</sub>. *Journal of Solid State Chemistry* **292**, 121743-121743 (2020).
20. I. Schewe-Miller, *Metallreiche Hauptgruppenmetall-Chalkogenverbindungen: Synthese, Strukturen und Eigenschaften.* (na, 1990).
21. J. Rodríguez-Carvajal, Recent advances in magnetic structure determination by neutron powder diffraction. *Physica B: Condensed Matter* **192**, 55-69 (1993).
22. P. Wikus, W. Frantz, R. Kümmerle, P. Vonlanthen, Commercial gigahertz-class NMR magnets. *Superconductor Science and Technology* **35**, 033001 (2022).
23. R. K. Harris, E. D. Becker, S. M. C. De Menezes, R. Goodfellow, P. Granger, NMR nomenclature: Nuclear spin properties and conventions for chemical shifts - IUPAC recommendations 2001. *Solid State Nuclear Magnetic Resonance* **22**, 458-483 (2002).
24. C. Lin *et al.*, Crystallization behavior of 80GeS<sub>2</sub> · 20Ga<sub>2</sub>S<sub>3</sub> chalcogenide glass. *Applied Physics A* **97**, 713-720 (2009).
25. M. Rozé *et al.*, Optical and Mechanical Properties of Glasses and Glass-Ceramics Based on the Ge-Ga-Se System. *Journal of the American Ceramic Society* **91**, 3566-3570 (2008).
26. A. Yang *et al.*, Ga-Sb-S Chalcogenide Glasses for Mid-Infrared Applications. *Journal of the American Ceramic Society* **99**, 12-15 (2016).
27. A. Lecomte, V. Nazabal, D. Le Coq, L. Calvez, Ge-free chalcogenide glasses based on Ga-Sb-Se and their stabilization by iodine incorporation. *Journal of Non-Crystalline Solids* **481**, 543-547 (2018).



## Data availability

View Article Online  
DOI: 10.1039/D6DT00232C

The data supporting this article are available within the article, in the supplementary information (SI) and from the corresponding author upon request.

